15th Australasian Fluid Mechanics Conference
The University of Sydney, Sydney, Australia
13-17 December 2004

Flow past a Cylinder with Free Hemispherical Ends: Comments on Grid Independence and Wake Symmetry Characteristics

G. J. Sheard[1], Mark C. Thompson[1] and K. Hourigan[1]

[1]Fluids Laboratory for Aeronautical and Industrial Research (FLAIR)
Department of Mechanical Engineering, Monash University, VIC 3800, AUSTRALIA

Abstract

A grid independence study and numerical computations are reported for the flow past cylinders with free hemispherical ends. A novel modelling technique is used whereby a spectral-element method is employed with an azimuthal Fourier expansion around the symmetry axis of the cylinder. The flow direction is then normal to the axis of symmetry, rather than in the axial direction. For benchmarking purposes, results using the proposed grids are compared to accurate computations of the flow past a sphere, and an accuracy of better than 0.5% is obtained up to a Reynolds number $Re = 300$. Plots showing alterations in the symmetry characteristics of the wakes are provided for length ratios up to $L_R = 10$.

Introduction

In this paper the suitability of a spectral-element method with an azimuthal Fourier expansion to study the flow past a cylinder with hemispherical ends (hereafter referred to simply as a "cylinder") is considered.

The cylinder may be described by a ratio between its overall length L, and its diameter d, giving the length ratio parameter $L_R = L/d$. Clearly then, $L_R = 1$ describes a sphere, whereas as $L_R \to \infty$, the straight circular span of the cylinder becomes the dominant geometric feature, and the flow properties should approach those of a straight circular cylinder. This paper considers only the case where the flow is normal to the symmetry axis of the cylinder. A Reynolds number is defined as $Re = U_\infty d/\nu$, based on the cylinder diameter d, the freestream velocity U_∞ and the kinematic viscosity of the fluid ν. A schematic diagram that shows the relevant dimensions of the cylinder is provided in figure 1.

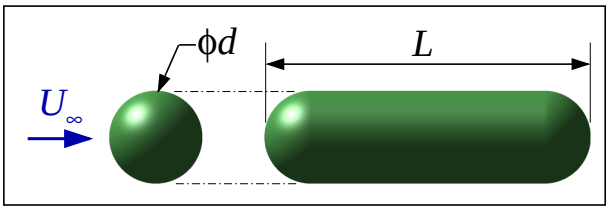

Figure 1: Schematic diagram showing the relevant dimensions of a cylinder with free hemispherical ends, and the relative direction of flow.

The low-Reynolds-number transitions for a sphere and a circular cylinder are somewhat different: [6] describes how the steady separated wake behind a circular cylinder becomes unsteady through a Bénard–von Kármán instability at approximately $Re = 47$ based on the cylinder diameter, and [16, 17, 18] describes the subsequent development of three-dimensional spanwise-periodic instabilities in the wake, beginning with the Mode A instability at approximately $Re = 180$. For a sphere, [15, 3] provided accurate measurements of a regular transition to a steady non-axisymmetric wake at $Re \approx 212$, and [2, 14] have shown that the subsequent transition to unsteady flow occurs at $Re \approx 272$ through a continuous supercritical bifurcation.

Short cylinders with hemispherical ends have been the subject of experimental studies in recent years [10, 7], driven largely by an interest in the variation in the transition Reynolds number for the development of unsteady flow, the subsequent variation in Strouhal frequency of shedding, and the interaction of wakes behind pairs of bluff bodies [9, 8]. The study of cylinders with hemispherical ends is also relevant to the study of circular cylinders of low aspect ratio (length/diameter) [5, 4]. In [10] the critical Reynolds numbers for the development of periodic flow in the wake behind cylinders with free hemispherical ends was measured for a range of cylinders $0 \leq L_R \leq 5$. They observe that the critical Reynolds number was approximately $Re_c = 270$ for a sphere ($L_R = 1$), and decreased with an increase in length ratio. At $L_R = 5$ a critical Reynolds number $Re_c \approx 85$ was measured. This value is still significantly higher than the value for a straight circular cylinder ($Re \approx 47$) measured by [6], suggesting that longer length ratios need to be considered. A benefit of the present numerical formulation is the ease with which larger length ratios can be modeled. The significant difference in flow properties between a cylinder with $L_R = 5$ and a straight circular cylinder can also be perceived from the measured Strouhal–Reynolds number profiles provided in [10, 7]. The Strouhal–Reynolds number profile for the cylinder with $L_R = 5$ initiates at the critical Reynolds number $Re_c \approx 85$ with a shedding frequency $St \approx 0.095$. This is approximately 21% below the Strouhal frequency at the critical Reynolds number for the onset of unsteady flow ($St \approx 0.12$) in the wake of a straight circular cylinder, and approximately 41% below the Strouhal frequency at the same Reynolds number.

Whereas the previous experimental studies have provided substantial data relating to the Strouhal–Reynolds number relationships for cylinders with $1 \leq L_R \leq 5$, little flow visualisation has been provided. The present numerical study will add significantly to our understanding of the structure of the flows following the development of unsteady and spanwise-asymmetric flow.

Numerical Formulation

The spectral-element scheme used in this study has been successfully applied to model the flow past axisymmetric bodies such as a sphere [14] and rings [11, 13]. These references should be consulted for further details of the numerical method.

The method employed here uses the same Fourier expansion of the velocity and pressure fields about an axis of symmetry as in the previous studies, but with the important distinction in that the flow direction is now normal to the axis of symmetry, rather than in the axial direction. The mesh required to adequately resolve the wake using this method has some unavoidable inherent inefficiencies. The use of a Fourier expansion of the flow field around the cylinder requires that a large number of Fourier planes be used to resolve details in the flow across the wake. In addition, the computational domain must extend sufficiently

far from the cylinder to minimise both transverse blockage effects, and the deterioration of the wake structure in the vicinity of the downstream domain. Using previous numerical studies as a guide [1, 14], a family of meshes was constructed that varied only in terms of the addition of elements between the hemispherical ends to model the cylinder span. The mesh employed to model a cylinder with $L_R = 1$ did not require any of these additional elements as the straight-span section of the cylinder had zero length. The meshes consistently employed 10 elements in the radial direction, and 5 elements between the axis and the straight span section around the cylinder ends. As an example, a plot of the mesh employed to model a cylinder with $L_R = 5$ is provided in figure 2.

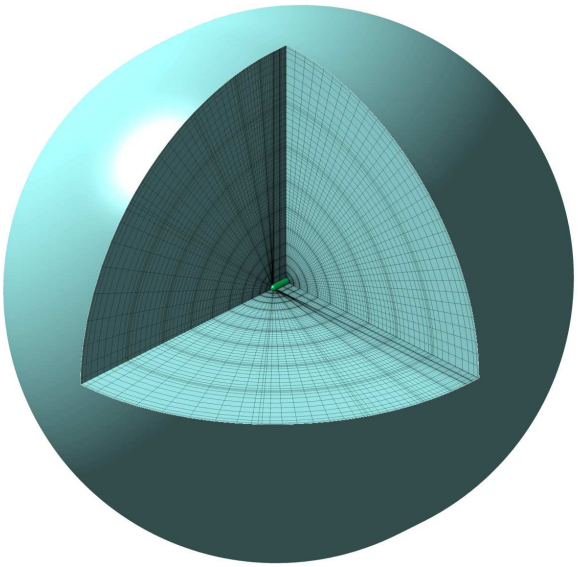

Figure 2: A cutaway view of the computational domain showing the mesh employed to model the flow past a cylinder with free hemispherical ends and a length ratio $L_R = 5$. Sub-elements are shown, and the domain extends $30d$ from the cylinder.

A grid independence study was performed at $Re = 300$ using the $L_R = 1$ mesh to allow comparison with previous sphere studies. Meshes with $P = 64$ and 128 Fourier planes were tested, to determine the number of planes required to resolve the wake, and the number of nodes per element was varied from $N^2 = 25$ to 144. The graph in figure 3 shows the convergence characteristics with increasing number of mesh nodes (N^2P) for the simulations with 64 and 128 planes. Notice that with 64 planes, the pressure and viscous components of the drag coefficient seem to converge to within a few percent of the accurate sphere computations (repeated from an earlier study [13]) indicated by the dotted lines, but the Strouhal frequency is 7% higher. This discrepancy indicates that 64 planes is insufficient to resolve the wake. Notice that with 128 planes, each of the parameters converges to within 0.5% of the accurate numerical values. Based on these findings, the meshes employed for this study each employed $P = 128$ planes, and $N^2 = 121$ nodes per element.

To improve the stability of the time-integration of the computations, a filter was applied to the azimuthal Fourier modes to reduce the number of modes in the vicinity of the axis of symmetry ($r \to 0$). This treatment reduces the limiting effect of the Courant condition on the time-step Δt.

Sphere Wake Comparison

A visual comparison of the wakes behind a sphere at $Re = 300$ computed using the present crossflow mesh and previous axial-flow meshes is provided in figure 4. Notice that although the flow quantities have converged to a high degree of accuracy using the crossflow method, an appreciable loss of fine detail in the wake has occurred. Despite this, the convergence of the flow quantities in the previous section suggests that meaningful quantitative predictions of the flow regimes up to $Re \approx 300$ can be made.

To confirm that the accuracy predicted at $Re = 300$ extends to lower Reynolds numbers, components of the mean drag were computed. These values are compared to the accurate results from [11, 12] in figure 5.

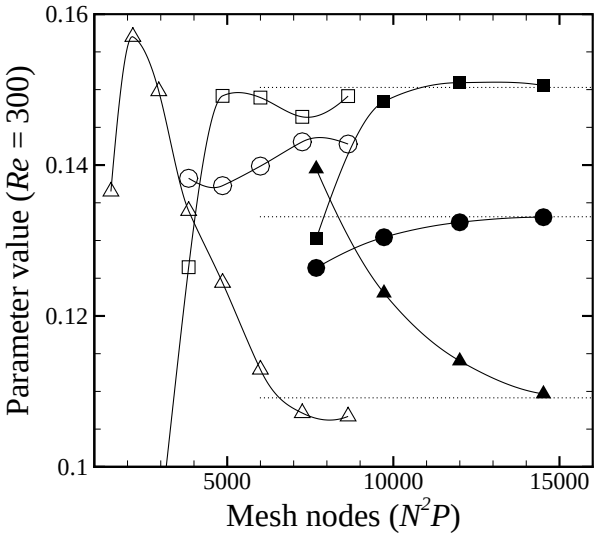

Figure 3: Convergence with increasing nodes per element (N^2) of a cylinder with $L_R = 1$ (a sphere) at $Re = 300$. Meshes with $P = 64$ and 128 planes (open and filled symbols, respectively) are investigated, and the parameters C_{D_p} (□), C_{D_v} (△) and St (◯) are monitored. The dotted lines show the corresponding parameter values from previous accurate studies of a sphere.

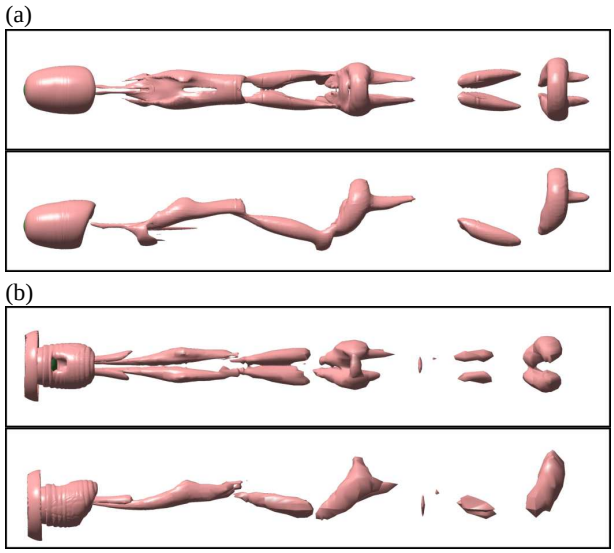

Figure 4: Isosurface plots showing the vortical structures in the wake behind a sphere. In (a), the wake is computed using the present crossflow grids, and in (b), a traditional axial-flow grid is used. The wake in each case is viewed from above and the side, and flow is from left to right.

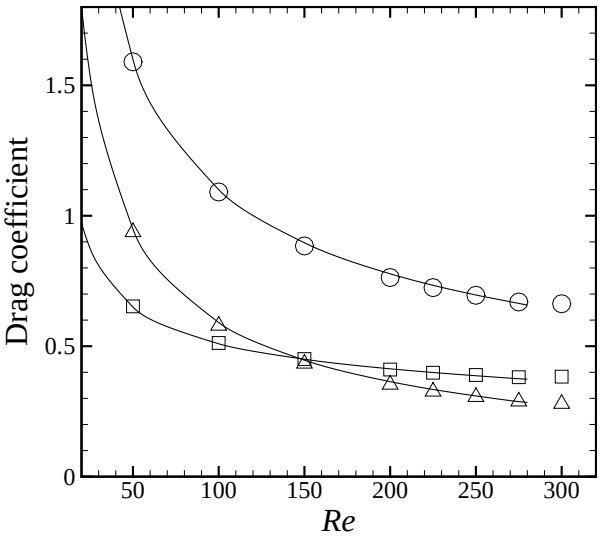

Figure 5: A comparison between the drag coefficient for a sphere using the present numerical technique (symbols), and from the accurate numerical computations of the flow by [11, 12] (lines). The mean pressure, viscous and total drag are shown by □, △ and ◯, respectively.

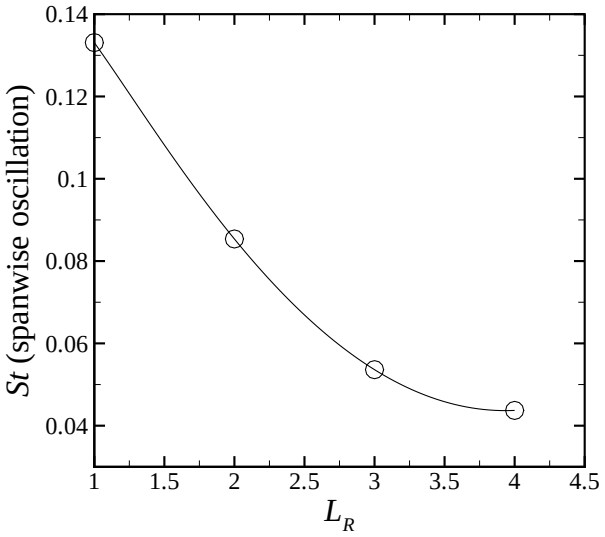

Figure 6: Strouhal frequency of the periodic oscillation in the spanwise body force at $Re = 300$. Variation with length ratio.

Cylinder with Hemispherical Ends at *Re* = 300

One of the primary goals of the present study is to determine how the hairpin shedding observed in the flow past a sphere relates to the Kármán vortex street behind a straight circular cylinder. The unsteady wakes behind cylinders with $L_R = 1$, 2, 3, 4 and 5 were computed at $Re = 300$. The variation in the pressure and viscous forces acting on the cylinders were monitored in three dimensions.

Chief among the interesting observations that have been made to date is the link between the frequency of the hairpin shedding from a sphere, and a spanwise oscillation computed in the flow past cylinders. The frequency of this oscillation decreases with an increase in L_R, as depicted in figure 6. The near-periodic oscillations became weaker in magnitude as the length ratio increased, and were replaced by a chaotic force response at $L_R = 5$. The decrease in the amplitude of the low-frequency oscillation in the spanwise direction contrasted a measured increase in the force response in the transverse direction normal to the plane of the wake. This fluctuation is thought to be consistent with the Kármán shedding process.

Included in figure 7 are isosurface plots showing the wakes behind cylinders with length ratios up to $L_R = 10$. The cylinders with length ratios in the range $0 \leq L_R \leq 5$ were computed at $Re = 300$, while the cylinder with $L_R = 10$ was computed at $Re = 100$. It can be seen that at smaller length ratios the wakes are not symmetrical about the cylinder mid-span. This asymmetry is associated with the Strouhal frequency of the spanwise component of force acting on the cylinder shown in figure 6. The development of a symmetry about the mid-span occurs between $L_R = 5$ and 10. This observed symmetry development with increasing length ratio is concurrent with the corresponding decrease in the strength of the spanwise force component.

Coinciding with the development of spanwise symmetry is the development of Kármán-like shedding in the vicinity of the cylinder mid-span, and within approximately 1d to 3d downstream. Evidence of this is shown by solid vertical bands in the isosurface plots, and can be seen in figure 7(d–f), although it is more pronounced at the larger length ratios shown in figure 7(e, f).

It is interesting to observe that even with a length ratio $L_R = 10$, the influence of the free hemispherical ends on the two-dimensional vortex street is significant. Downstream of the cylinder (to between 4d and 5d downstream), evidence of an approximately parallel vortex street can be observed. Further downstream, the rollers in the wake are deformed by the three-dimensional effects induced by the flow around the free hemispherical ends, and a symmetrical three-dimensional wake replaces the quasi-two-dimensional wake in the vicinity of the mid-span.

Conclusions

A novel implementation of a spectral-element method has been employed to model the flow past a cylinder with hemispherical ends. Computations of the flow past a sphere using the current crossflow implementation were compared with previous accurate numerical computations that used the more traditional axial-flow method. For comparison, isosurface plots, Strouhal frequencies and drag coefficients were monitored, and errors were within 0.5% throughout the Reynolds number range $Re \lesssim 300$. A limited number of computations of cylinders with length ratios in the range $1 \leq L_R \leq 5$ provide tantalising hints to the diverse flow regimes to be found.

Acknowledgements

This research is supported by an ARC Linkage International grant. These simulations were performed using the resources of the Victorian Partnership for Advanced Computing (VPAC) consortium.

References

[1] Barkley, D. and Henderson, R. D., Three-dimensional Floquet stability analysis of the wake of a circular cylinder, *J. Fluid Mech.*, **322**, 1996, 215–241.

[2] Ghidersa, B. and Dušek, J., Breaking of axisymmetry and onset of unsteadiness in the wake of a sphere, *J. Fluid Mech.*, **423**, 2000, 33–69.

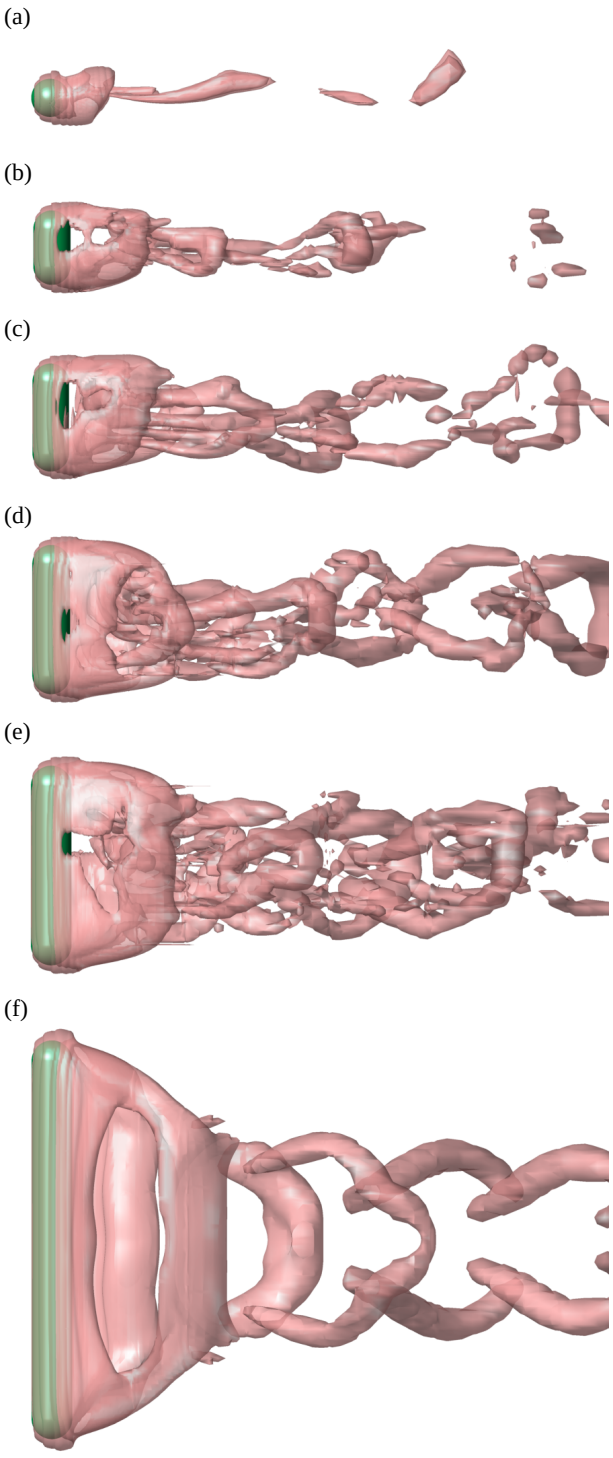

Figure 7: Isosurface plots of the vortical structure of the wakes behind cylinders with free hemispherical ends. Parts (a–e) show length ratios $L_R = 1$, 2, 3, 4 and 5, respectively, at $Re = 300$, and part (f) shows a length ratio $L_R = 10$ at $Re = 100$.

[3] Johnson, T. A. and Patel, V. C., Flow past a sphere up to a Reynolds number of 300, *J. Fluid Mech.*, **378**, 1999, 19–70.

[4] Ko, N. W. M., Law, C. W. and Lo, K. W., Mutual interference on transition of wake of circular cylinder, *Phys. Fluids*, **12**, 1962, 1–34.

[5] Norberg, C., An experimental investigation of the flow around a circular cylinder: Influence of aspect ratio, *J. Fluid Mech.*, **258**, 1994, 287–316.

[6] Provansal, M., Mathis, C. and Boyer, L., Bénard-von Kármán instability: Transient and forced regimes, *J. Fluid Mech.*, **182**, 1987, 1–22.

[7] Provansal, M., Schouveiler, L. and Leweke, T., From the double vortex street behind a cylinder to the wake of a sphere, *Euro. J. Mech. B (Fluids)*, **23**, 2004, 65–80.

[8] Schouveiler, L., Brydon, A., Leweke, T. and Thompson, M. C., Interactions of the wakes of two spheres placed side by side, **23**, 2004, 137–145.

[9] Schouveiler, L., Brydon, A., Leweke, T. and Tompson, M. C., Interaction of the wakes of two spheres placed side by side, in *Proceedings of the Conference on Bluff Body Wakes and Vortex Induced Vibrations (BBVIV3)*, editors K. Hourigan, T. Leweke, M. C. Thompson and C. H. K. Williamson, Published by Monash University, Melbourne, VIC 3800, Australia, Port Douglas, Australia, 2002.

[10] Schouveiler, L. and Provansal, M., Periodic wakes of low aspect ratio cylinders with free hemispherical ends, *J. Fluids Struct.*, **14**, 2001, 565–573.

[11] Sheard, G. J., *The Stability and Characteristics of the Flow Past Rings*, Ph.D. thesis, Monash University, Melbourne, Australia, 2004.

[12] Sheard, G. J., Hourigan, K. and Thompson, M. C., Quantitative computations of the drag coefficients for the low Reynolds number flow past rings, *Under consideration for publication in J. Fluid Mech.*.

[13] Sheard, G. J., Thompson, M. C. and Hourigan, K., From spheres to circular cylinders: Non-axisymmetric transitions in the flow past rings, *J. Fluid Mech.*, **506**, 2004, 45–78.

[14] Thompson, M. C., Leweke, T. and Provansal, M., Kinematics and dynamics of sphere wake transition, *J. Fluids Struct.*, **15**, 2001, 575–585.

[15] Tomboulides, A. G., Orszag, S. A. and Karniadakis, G. E., Direct and large-eddy simulation of the flow past a sphere, in *Proceedings of the Second International Conference on Turbulence Modeling and Experiments (2nd ICTME)*, Florence, Italy, 1993.

[16] Williamson, C. H. K., Defining a universal and continuous Strouhal-Reynolds number relationship for the laminar vortex shedding of a circular cylinder, *Phys. Fluids*, **31**, 1988, 2742–2744.

[17] Williamson, C. H. K., The existence of two stages in the transition to three-dimensionality of a cylinder wake, *Phys. Fluids*, **31**, 1988, 3165–3168.

[18] Williamson, C. H. K., Mode A secondary instability in wake transition, *Phys. Fluids*, **8**, 1996, 1680–1682.